

Mapping of bioluminescent images onto CT volume surface for dual-modality BLT and CT imaging

Xueli Chen^{a,b}, Jimin Liang^{a,*}, Xiaochao Qu^a, Yanbin Hou^a, Shouping Zhu^a, Duofang Chen^a, Xinbo Gao^b and Jie Tian^{a,c,*}

^aSchool of Life Sciences and Technology, Xidian University, Xi'an, Shaanxi, China

^bSchool of Electronic Engineering, Xidian University, Xi'an, Shaanxi, China

^cInstitute of Automation, Chinese Academy of Sciences, Beijing, China

Received 30 June 2011

Revised 27 September 2011

Accepted 18 October 2011

Abstract. We present a method for mapping the two-dimensional (2D) bioluminescent images (BLIs) onto a three-dimensional (3D) body surface derived from the computed tomography (CT) volume data. This mapping includes two closely-related steps, the spatial registration of the 2D BLIs into the coordinate system of the CT volume data and the light flux recovering on the body surface from BLIs. By labeling markers on the body surface, we proposed an effective registration method to achieve the spatial position alignment. The subsequent light flux recovering is presented based on the inverse process of the free-space light transport model and taking the influence of the camera lens diaphragm into account. Incorporating the mapping procedure into the bioluminescence tomography (BLT) reconstruction, we developed a dual-modality BLT and CT imaging framework to provide both optical and anatomical information. The accuracy of the registration and the light flux recovering methods were evaluated via physical phantom experiments. The registration method was found to have a mean error of 0.41 mm and 0.35 mm in horizontal and vertical direction, and the accuracy of the light flux recovering method was below 5%. Furthermore, we evaluated the performance of the dual-modality BLT/CT imaging framework using a mouse phantom. Preliminary results revealed the potential and feasibility of the dual-modality imaging framework.

Keywords: Dual-modality imaging, bioluminescence tomography (BLT), computed tomography (CT), spatial registration, light flux recovering

1. Introduction

As a promising non-contact optical imaging technology, bioluminescence tomography (BLT) has received increased attention in recent years [1]. By integrating multi-angle bioluminescent images (BLIs), geometrical structures and tissue optical properties, BLT aims to reconstruct the bioluminescent probe distribution inside a small living animal based on an accurate light transport model [2]. However, BLT only macroscopically reflects the physiological and pathological activities of the tumorous tissues

*Corresponding author: Jimin Liang, School of Life Sciences and Technology, Xidian University, Xi'an, Shaanxi 710126, China. Tel.: +86 29 81891016; Fax: +86 29 81891070; E-mail: jimleung@mail.xidian.edu.cn.

inside an animal's body, but cannot provide structural information of the internal organs. Thus, it needs to be registered with the anatomical structure to determine the probe position [3,4]. In 2003, Wang first presented the concept of BLT and developed the corresponding imaging system prototype [5]. On the basis of the prototype system, reconstruction algorithm was developed by fusing the anatomical structure acquired by computed tomography (CT) and applied to *in vivo* small animal studies [6]. After that, fusing the anatomical structure obtained from CT or magnetic resonance imaging to reconstruct the internal bioluminescent probe distribution has become a dominating branch of BLT [3,4,7–10]. However, the past researches have not achieved a seamless integration at the system level and the fusion of the bioluminescent and structural information is implemented by using complicated registration algorithms [3,4].

The input data for source reconstruction in BLT are the two-dimensional (2D) BLIs acquired by the non-contact CCD camera. However, the existing source reconstruction algorithms are all based on the light flux distribution on the body surface [11–17]. Thus, it is necessary to map the 2D BLIs onto the three-dimensional (3D) body surface derived from the anatomical structure. Based on the Lambertian source theory of diffuse light, we have proposed two types of free-space light transport models, which are used to describe the light transport process from the body surface to the CCD camera [18,19]. At the same time, motivated by the principle of the optical path reversibility and the ideology of the reciprocity theorem between sources and detectors, we have developed an effective method for the recovering of the surface light flux distribution from the multi-angle 2D BLIs [20]. Our light flux recovering method is based on the following two assumptions. Firstly, the anatomical structure has been obtained by the structural imaging modalities beforehand. Secondly, the 2D BLIs have been registered into the coordinate system of the structural volume. There is no absolutely physical coordinate for the 2D BLIs and the anatomical structure used in the bioluminescent source reconstruction is originated from the volume of the CT reconstruction. Therefore, before performing the surface light flux recovering, we should first determine the position of the BLIs in the coordinate system of the CT volume data. Furthermore, our previous light flux recovering method did not consider the influence of the camera lens diaphragm which imposes great impact on the detection results [19]. As a result, if the influence of the camera lens diaphragm is considered in the light flux recovering procedure, the mapping results of 2D BLIs onto the 3D body surface may be further improved.

In this paper, we proposed a new method for mapping 2D BLIs onto a 3D body surface derived from the CT volume. This mapping includes two closely-related steps, the spatial registration of the 2D BLIs into the coordinate system of the CT volume data and the light flux recovering on the body surface from 2D BLIs. By labeling markers on the body surface, an effective registration method was presented to achieve the alignment of spatial position which is to determine the position of the BLIs in the coordinate system of the CT volume data. The presented registration method is based on the seamless integration of BLT and CT at the system level, and is specified for the subsequent light flux recovering procedure. Moreover, considering the influence of the camera lens diaphragm, we improved our previously proposed light flux recovering method [20]. Incorporating the mapping procedure into BLT reconstruction, we developed a dual-modality BLT and CT imaging framework to provide both optical and anatomical information. The accuracy of the registration procedure and the improvement of the light flux recovering method were evaluated via physical phantom experiments. In addition, we also investigated and discussed the influence of the registration error on the subsequent surface light flux recovering and the internal bioluminescent source reconstruction. Finally, the performance of the dual-modality BLT/CT imaging framework was evaluated by using a mouse phantom. Preliminary results revealed the potential and feasibility of the dual-modality imaging framework.

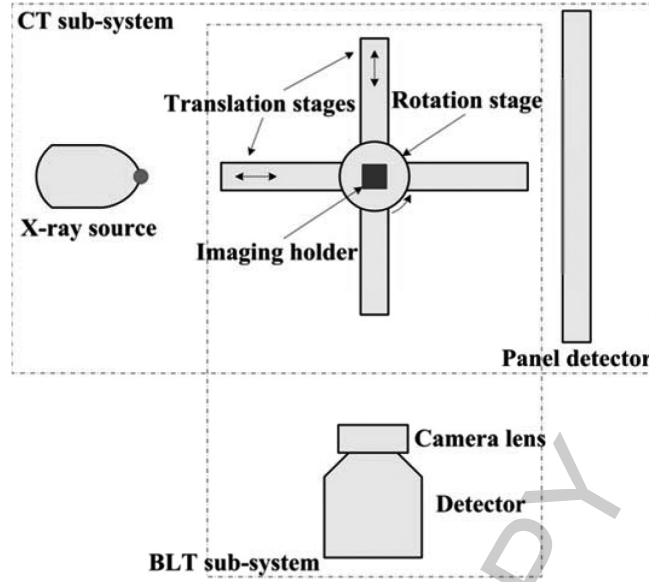


Fig. 1. Schematic diagram for dual-modality BLT/CT imaging system.

2. Mapping of 2D bioluminescent images onto a 3D body surface

2.1. Spatial registration of the 2D BLIs into the coordinate system of the CT volume data

To perform the dual-modality BLT/CT imaging, we developed a seamlessly integrated system that is composed of the BLT prototype sub-system and micro-CT sub-system [21]. In the dual-modality system, two subsystems are fixed perpendicularly and share a control system, including the translation stages, rotation stage and imaging holder. The imaging holder is fixed on the rotation stage, and the rotation stage is placed on the translation stages as shown in Fig. 1. Since the 0^0 view image is in the same position for both the 2D BLIs and micro-CT projection image, the surface markers in the identical perspective of the two images have the same physical coordinates. In the existing BLT technologies, four- or single view BLIs are commonly utilized for the internal source reconstruction. Considering the perpendicular layout of the two subsystems at the same time, we assume that the BLIs are perpendicularly located at the X- or Y-axis of the coordinate system of the CT volume data. Furthermore, variation trends for the physical coordinates of each pixel on the BLIs are static and the same as those in the coordinate system of the CT volume data. Thus, as long as we determine the physical coordinates of the central position of BLIs in the coordinate system of the CT volume data, the physical coordinates of all of the pixels can be calculated according to the variation trends. Thus, the registration in this paper is to calculate the physical coordinates of the central position of BLIs based on the surface markers.

Because the BLI is perpendicularly located at the X- or Y-axis of the coordinate system of the CT volume data, we just need to register the non-axial coordinate of the central position of each BLI. The axial coordinate of the central position can be calculated according to the lens law and the location of the imaging holder in the experiments. Therefore, given the physical coordinates, the CT slice coordinates and the BLT pixel coordinates of the surface markers, the central coordinates of the BLIs can be determined using the following formula:

$$\begin{aligned}x_c &= -\eta(1-\sigma) + \sigma[r_x x_m^{CT} + \eta l_x(x_m^{BLI} - x_c^{BLI})] \\y_c &= -\eta\sigma + (1-\sigma)[r_y y_m^{CT} + (-\eta)l_y(y_m^{BLI} - y_c^{BLI})] \\z_c &= r_z z_m^{CT} + l_z(z_m^{BLI} - z_c^{BLI})\end{aligned}\quad (1)$$

where (x_c, y_c, z_c) are the registered central coordinates of the BLI; (r_x, r_y, r_z) is the slice resolution of the CT volume in the axial direction; $(x_m^{CT}, y_m^{CT}, z_m^{CT})$ are the slice coordinates of the surface marker in the CT volume data; $(x_m^{BLI}, y_m^{BLI}, z_m^{BLI})$ are the pixel coordinates of the surface marker in the BLIs; $(x_c^{BLI}, y_c^{BLI}, z_c^{BLI})$ are the pixel coordinates of the center in the BLI; (l_x, l_y, l_z) is the optics magnification along the axial direction on the virtual detection plane [18–20]; and η and σ are defined as the identifier functions which are used for identifying the axis of the BLIs located with their definition as:

$$\sigma = \begin{cases} 0 & I \perp X\text{-axis} \\ 1 & I \perp Y\text{-axis} \end{cases} \quad (2)$$

$$\eta = \begin{cases} -1 & I \in \text{positive axis} \\ 1 & I \in \text{negative axis} \end{cases} \quad (3)$$

where I represents the BLIs. In Eq. (1), (x_c, y_c, z_c) are the coordinates in the BLI physical coordinate system, $(x_m^{CT}, y_m^{CT}, z_m^{CT})$ are the ones in the CT system, $(x_m^{BLI}, y_m^{BLI}, z_m^{BLI})$ and $(x_c^{BLI}, y_c^{BLI}, z_c^{BLI})$ are the ones on the BLI image system. Therein, the BLI physical coordinate system is defined the same as the CT system.

Rearranging Eq. (1), we obtain the following matrix equation:

$$\mathbf{R} = \mathbf{C} + \mathbf{MA} + \mathbf{DB} \quad (4)$$

where $\mathbf{R} = [x_c, y_c, z_c]^T$ is a column vector which is comprised of the registered central coordinate of the BLIs; $\mathbf{C} = [-\eta(1-\sigma), -\eta\sigma, 0]^T$ is the identifier function vector; \mathbf{M} is a column vector that is formed by the physical coordinates of the surface marker and satisfies $\mathbf{M} = [r_x x_m^{CT}, r_y y_m^{CT}, r_z z_m^{CT}]^T$; $\mathbf{A} = [\sigma, 1-\sigma, 1]$ is a constant coefficient vector that is used to identify which axis the bioluminescent image is located on; $\mathbf{D} = [l_x(x_m^{BLI} - x_c^{BLI}), l_y(y_m^{BLI} - y_c^{BLI}), l_z(z_m^{BLI} - z_c^{BLI})]^T$ is the optical distance vector along the axial direction between the surface marker and the center of the BLIs; and \mathbf{B} is the constant coefficient vector of the optical distance and denotes $\mathbf{B} = [\eta\sigma, \eta(1-\sigma), 1]$.

Since the dual-modality BLT/CT imaging system is seamlessly integrated by being fixed perpendicularly and sharing a control system, we can ensure that the 0^0 view image is in the same position for both the 2D BLIs and micro-CT projection image. Thus, if the physical coordinates of surface markers in the coordinate system of the CT volume data, the slice coordinates of the surface markers in the CT volume data, the pixel coordinates of the surface markers in the BLIs and the axial optics magnification have been given, we can register the 2D BLIs into the coordinate system of the CT volume data using Eq. (4).

2.2. Light flux recovering on the body surface from 2D BLIs

Motivated by the principles of optical path reversibility and the ideology of the reciprocity theorem between sources and detectors, each pixel of the BLIs is assumed as a Lambertian source, eradiating light power to the surface of the body. Based on the Lambertian source theory of diffuse light, we have proposed a light flux recovering method for the reconstruction of light flux distribution on the body surface from multi-view 2D BLIs [20]. However, this method only worked well for the case of the large

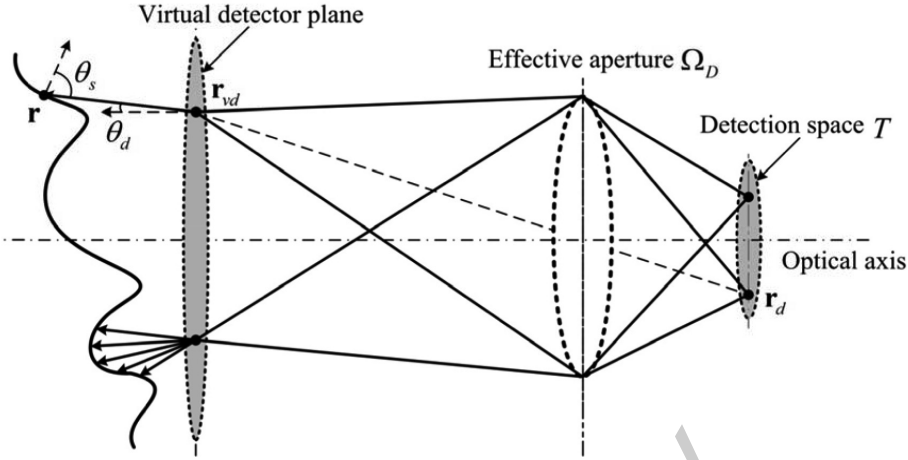


Fig. 2. Diagram for the procedure of the surface light flux recovery and descriptions of the related parameters.

aperture camera lens because the influences of the camera lens diaphragm were not considered. In our previous study [19], we have incorporated these effects into modeling the light transport from the body surface to the CCD camera by improving the visibility factor. In this paper, we improved our light flux recovering method using the improved visibility factor. Thus, corresponding relationship between the outward flux at any point of the body surface and the light power in the acquired BLIs is obtained:

$$J(r) = \frac{1}{\pi} \int_T E(r_d) \alpha(r_{vd}, r) \beta(r_d, r; \Omega_D) \frac{\cos \theta_s \cos \theta_d}{|r - r_{vd}|} dT \quad (5)$$

where $J(r)$ is the outward flux at point r of the body surface; T is the detection space constructed by all of the pixels in the bioluminescent image; $E(r_d)$ is the light power received at point r_d of the detection space; r_{vd} is the imaging point of r_d on the virtual detector plane; θ_s is the included angle between the unit direction vector from r_{vd} to r and the normal vector of the surface point r ; θ_d is the included angle between the unit direction vector and the normal vector of the virtual detector point r_{vd} ; $\alpha(r_d, r)$ is the field visibility factor and $\beta(r_d, r; \Omega_D)$ is the effective visibility factor, which are generalized from the analysis of the camera lens diaphragm as presented in [19] and are used to determine whether the energy mapping relationship exists between the two points; and Ω_D represents the size of effective aperture and is dependent on the camera lens diaphragm. The detailed derivation of Eq. (5) can refer to the literatures [19,20], and the diagram for the procedure of the surface light flux recovery and descriptions of the related parameters are intuitively described in Fig. 2.

3. Dual-modality BLT/CT imaging framework

Based on the dual-modality BLT/CT imaging system, we have developed a dual-modality BLT/CT imaging framework by integrating the mapping of 2D BLIs onto the 3D body surface into the internal bioluminescent source reconstruction procedure. The whole procedure of the dual-modality imaging framework is shown in Fig. 3. Some important procedures are presented in detail as follows.

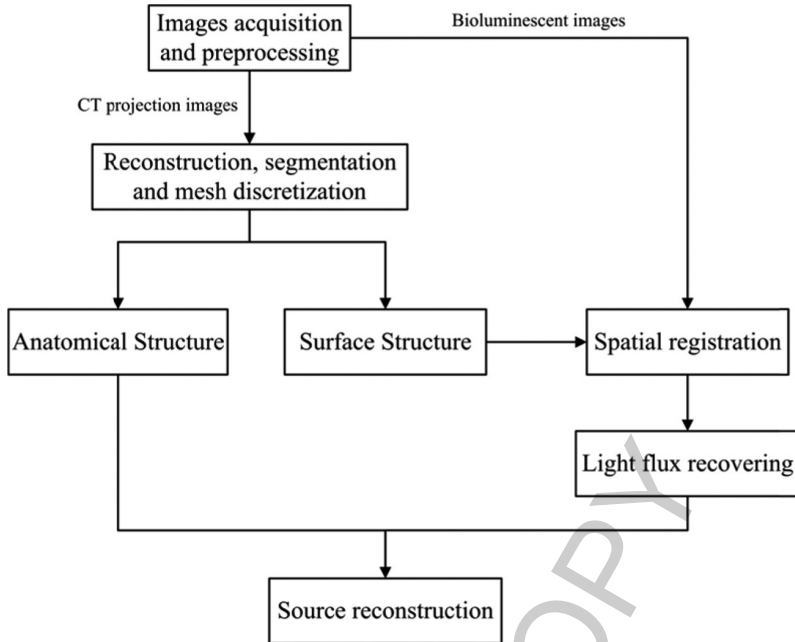


Fig. 3. Procedures of the dual-modality BLT/CT imaging framework.

3.1. Dual-modality images acquisition and preprocessing

Controlling the translation stages via software, we adjust the imaging holder and ensure its location at the perpendicular center of the two sub-systems. The imaging holder is ensured to be imaged clearly at the CCD camera by adjusting the BLT sub-system. By space-equally rotating the rotation stage three 90° in an anticlockwise direction, four views of bioluminescent images and marker-labeled photographs are acquired using the BLT sub-system. Subsequently, 480 views of CT projection images are acquired by the micro-CT sub-system by space-equally rotating the rotation stage 0.75° .

After acquiring the experimental data using the dual-modality BLT/CT imaging system, the images have to be preprocessed. By reconstructing the preprocessed CT projection images, we obtain the CT volume data using the GPU accelerated FDK algorithm [22]. The main organs are then segmented to form the 3D anatomical structure of the body [23]. To provide the volume surface for mapping of BLIs onto the CT volume data and the tetrahedral mesh for the reconstruction of the internal bioluminescent source, we discretize the CT volume data using the software of AmiraTM (Mercury Computer Systems, MA).

3.2. Spatial registration of the 2D BLIs into the coordinate system of the CT volume data

The registration process is realized based on the following procedures. Firstly, the slice coordinates of the surface markers are extracted from the reconstructed CT volume data and the pixel coordinates are obtained from the 2D BLIs. Secondly, based on the slice coordinates and the axial resolution utilized in the volume reconstruction, we calculate the corresponding physical coordinates M in the coordinate system of the CT volume data. Thirdly, after experimentally determining the axial optics magnification, we achieve the axial optical distance vector D. Lastly, by substituting the afore-cited information into Eq. (4), we obtain the physical coordinate vector R of the 2D BLIs in the coordinate system of the CT volume data.

3.3. Light flux recovering on the body surface from 2D BLIs

After obtaining the physical coordinates of the central position of the BLIs in the coordinate system of the CT volume data, the physical coordinates of all of the pixels can be determined based on the variation trends of the axial coordinates. Thus, the alignment of spatial positions between the BLIs and the body surface can be established. Then, the energy mapping from the BLIs to a point on the body surface can be constructed using Eq. (5). After further integration of Eq. (5) over the whole body surface, we can obtain the recovered light flux distribution on the body surface.

3.4. Reconstruction of the internal bioluminescent source

Bioluminescence probes, such as Fluc, emit bioluminescent light with a peak wavelength at red and near-infrared ranges in which the spectrum of the biological tissues are scattering dominated. Thus, the diffusion equation and Robin boundary condition are commonly used in BLT [11–17]:

$$\begin{aligned} -\nabla \cdot (D(r)\nabla\Phi(r)) + \mu_a(r)\Phi(r) &= S(r)(r \in \Omega) \\ \Phi(r) + 2A_n(r)D(r)(v(r) \cdot \nabla\Phi(r)) &= 0(r \in \partial\Omega) \end{aligned} \quad (6)$$

where $\Omega \in \mathbb{R}^3$ denotes the whole solving domain; r is an arbitrary position vector in the domain Ω ; $\Phi(r)$ is the nodal flux density at position r ; $S(r)$ represents the power density of the bioluminescent source; $\mu_a(r)$ is the absorption coefficient; $D(r)$ is the diffusion coefficient and satisfies $D(r) = [3(\mu_a + \mu'_s)]^{-1}$, where μ'_s is the reduced scattering coefficient; $A_n(r)$ is the mismatch factor of the refractive index; and $v(r)$ is the outward unit normal vector on the boundary $\partial\Omega$.

In the dual-modality BLT/CT imaging framework, the finite element method (FEM) is adopted to discretize Eq. (6). Thus, a linear matrix equation that links the unknown internal light source and the surface measured light flux density is established:

$$AS^{Per} = \Phi^B \quad (7)$$

where S^{Per} represents the unknown light source distribution located in the potential source region that is determined by an *a priori* knowledge or the reconstructed outward light flux distribution on the body surface; A is the system matrix that removes the rows corresponding to the interior nodes; and Φ^B denotes the nodal flux density on the boundary of the domain and satisfies $\Phi^B(r) = 2A_n(r)J(r)$, where $J(r)$ is the reconstructed outward light flux on the body surface.

Considering the severe ill-posedness of the source reconstruction problem, it is impossible to obtain the unknown source distribution from Eq. (7) directly. Usually, Eq. (7) is regularized to the following regularization problem:

$$\min \|AS^{Per} - \Phi^B\|_{\wedge} + \lambda \|S^{Per}\|_{\wedge} \quad (8)$$

where λ is the regularization factor determined by experiments or the L-curve method [24]. In the experimental section, an adaptive hp -FEM algorithm combined with l_2 norm based Tikhonov regularization is used to evaluate the developed dual-modality BLT/CT imaging framework. Using the modified Newton method with an active set strategy [16], we obtain the unknown bioluminescent source distribution.

Table 1

Comparisons between the actual and the registered physical coordinates of the central position of the bioluminescent images (in units of mm)

	Actual central position	Registered central position	Registration error	Average error
x positive axis	(19.600, 14.296)	(20.093, 13.793)	(0.493, 0.503)	(0.412, 0.347)
x negative axis	(21.106, 14.296)	(20.661, 14.044)	(0.445, 0.252)	
y positive axis	(21.268, 13.919)	(21.314, 13.713)	(0.046, 0.206)	
y negative axis	(19.635, 14.422)	(20.297, 13.994)	(0.662, 0.428)	

Note: x positive axis represents that the bioluminescent image is perpendicular to the x positive sub-axis, and the others are similar.

4. Experiments and results

In this section, four groups of verification experiments were designed and conducted to validate the accuracy of the surface marker based spatial registration method, and to evaluate the performance of the improved light flux recovering method and the dual-modality BLT/CT imaging framework. Firstly, a cylinder phantom based experiment was performed to validate the accuracy of the proposed spatial registration method under the assumption that the actual physical coordinates of the central position of the BLIs had been pre-obtained. Then, we investigated the influence of the registration error on the recovering of the surface light flux distribution. Lastly, the performance of the improved light flux recovering method and the dual-modality imaging framework were evaluated with a mouse phantom.

4.1. Accuracy validation of the spatial registration method

In this sub-section, a nylon cylindrical phantom of 30 mm diameter and 30 mm height was designed and utilized to perform the accuracy validation experiment. In the bioluminescent imaging experiment, a luminescent solution with a peak wavelength at about 650 nm was selected to simulate the internal bioluminescent source. To place the bioluminescent sources, two small holes of 1 mm radius and 5 mm center to center distance were drilled with a distance of 9 mm away from the phantom center. Prior to the imaging experiment, small balls made of plasticine were adhered to the phantom surface and utilized as surface markers. After adjusting the dual-modality BLT/CT imaging system based on the procedure presented in Section 3.1, four views BLIs, four views photographs with markers, and 480 views CT projection images were acquired and preprocessed. In the procedure of adjusting the dual-modality imaging system, the center of the phantom in the photographs was ensured to be at the center of the image. Therefore, the actual physical coordinates of the central position of the BLIs that were required to be registered were the center of the phantom in the corresponding view image.

Table 1 presents the comparisons between the actual and the registered physical coordinates of the central position of the BLIs. Based on the comparison results, we find that the registration errors in the horizontal direction were slightly larger than those in the vertical direction. For example, the worst error in the horizontal direction was up to 0.662 mm, but the value was 0.503 mm in the vertical direction. This was mainly caused by the fact that the optics magnification in the horizontal direction was not the same as that in the vertical direction. In bioluminescence imaging, because the depth of field effects exists in the imaging system, not all of the points on the body surface are imaged exactly on the CCD camera. Thus, the optics magnification is different for the different surface points. Particularly, the fluctuation becomes larger for curved surface. As a result, the influence of the optics magnification on the registration results in the horizontal direction is larger than that in the vertical direction. However,

Table 2
Influence of registration error on the recovering of surface light flux distribution

Registration error	0.5	0.6	0.7	0.8	0.9	1.0	1.1	1.2	1.5	2.0
Recovered error	0.014	0.019	0.022	0.022	0.022	0.025	0.029	0.031	0.035	0.045

the accuracy of the proposed spatial registration method is acceptable from the aspect of the average registration error, with values being about 0.412 mm in the horizontal direction and 0.347 mm in the vertical direction, which are both less than 0.5 mm.

4.2. Influence of registration error on the recovering of surface light flux distribution

To investigate the influence of the registration error on the subsequent recovering of the surface light flux distribution, we artificially enlarged the registration error and then recovered the surface light flux distribution using the modified registration results. Based on the accuracy of the surface light flux distribution, we determined the maximum registration error that can be affordable. Here, the average registration error was set to be changed from 0.5 mm to 2 mm as listed in Table 2. Three curves were extracted from the phantom surface at the height of 15 mm, 19 mm and 23 mm. Then, we compared the recovered surface light flux distribution using the inaccurate registration results with that using the accurate one on the three curves, and defined their average difference as the error for the recovering of the surface light flux distribution (termed as the recovering error from now on). The recovering errors corresponding to different registration errors are listed in Table 2.

From Table 2, some interesting conclusions are addressed. Firstly, the recovering error becomes larger and larger as the registration error increases. Secondly, the recovering error is less than 3% if the registration error is no larger than 1.1 mm. Thus, we conclude that an acceptable recovered result of the surface light flux distribution can be obtained when the registration error is smaller than 1.1 mm. Furthermore, comparable reconstructed results of the internal bioluminescent source are obtained when the recovering error is less than 5%, as presented in [20]. Therefore, the registration error of the proposed registration method is acceptable for the subsequent recovering of the surface light flux distribution and the reconstruction of the internal bioluminescent source. Figure 4 presents the comparisons between the recovering of the surface light flux distribution using the registration results calculated by our proposed registration method and that using actual registration results. Therein, Fig. 4(a) shows the recovered surface light flux distribution based on the registration results calculated using the proposed registration method and corresponding recovered distribution based on the actual registration results is shown in Fig. 4(b); Fig. 4(c)–(e) present the curve comparisons at the height of 15 mm, 19 mm and 23 mm. From Fig. 4, we find that the recovered surface light flux distribution is slightly different in both cases, which further demonstrates the effectiveness of the proposed registration method.

4.3. Performance of the improved light flux recovering method and developed dual-modality BLT/CT imaging framework

To evaluate the performance of the improved light flux recovering method and the developed dual-modality BLT/CT image framework, a nylon mouse shape phantom was designed and manufactured to conduct the imaging experiment. A small hole of 1.5 mm radius was drilled at the head of the mouse phantom to locate the bioluminescent source where luminescent solutions of 20 μl volume were injected. The luminescent solutions were extracted from a red luminescent light stick (Glowproducts, Canada), with the peak emission wavelength at about 650 nm. In this wavelength, the optical properties of the

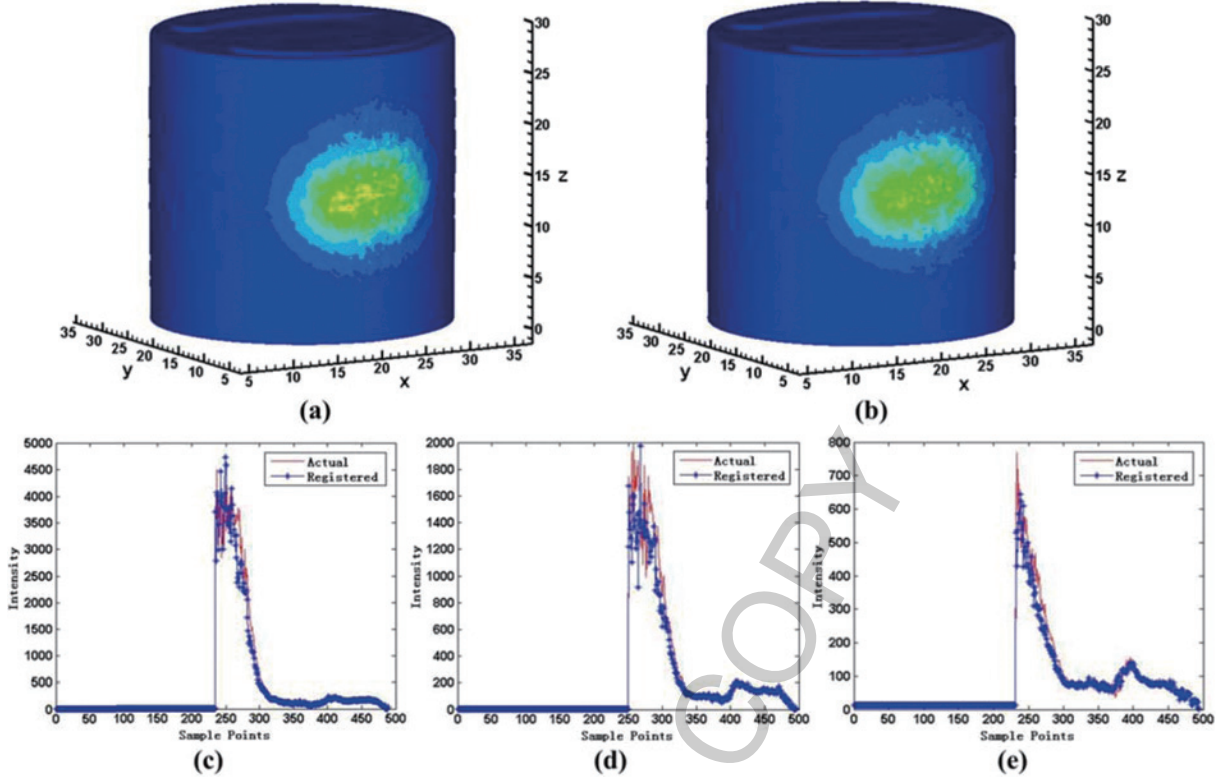


Fig. 4. Comparisons between the recovered surface light flux distribution using the registration results calculated by our proposed registration method and that using actual registration results. (a) Recovered surface light flux distribution based on the registration results calculated using the proposed registration method; (b) Recovered distribution based on the actual registration results; (c)–(e) Curve comparisons at the height of 15 mm, 19 mm and 23 mm.

phantom can be taken as: the absorption coefficient $\mu_a = 0.0138 \text{ mm}^{-1}$, and the reduced scattering coefficient $\mu'_s = 0.91 \text{ mm}^{-1}$. Similarly, small balls made of plasticine were also adhered to the surface of the mouse phantom prior to the experiment. After adjusting the dual-modality BLT/CT imaging system based on the procedure presented in Section 3.1, four views BLIs, four views photographs with markers, and 480 views CT projection images were acquired and preprocessed.

The information of the surface markers were first extracted from the preprocessed data, including the CT slice coordinates $(x_m^{CT}, y_m^{CT}, z_m^{CT})$ and the optical pixel coordinates $(x_m^{BLI}, y_m^{BLI}, z_m^{BLI})$, the pixel coordinates of the center of the BLIs $(x_c^{BLI}, y_c^{BLI}, z_c^{BLI})$, the slice resolution of the CT volume data (r_x, r_y, r_z) and the axial optics magnification (l_x, l_y, l_z) . Then, the physical coordinates of the central position of the BLIs in the coordinate system of the CT volume data were calculated using Eq. (4). Table 3 lists the registered results of the center of the BLIs into the coordinate system of the CT volume data. Based on the registered coordinates presented in Table 3, the preprocessed BLIs and the surface profile of the mouse phantom extracted from the CT volume data, the light flux distribution on the surface of the mouse phantom was recovered using our previous proposed and improved light flux recovering method respectively. To evaluate the improvement of the light flux recovering method, the recovered light flux distribution was compared with a simulation result using the Monte Carlo method [25]. Figure 5 presents the comparisons between the recovered light flux distribution and the simulation results, where Fig. 5(a)–(c) show the compared curves between the recovered result by our previous proposed method

Table 3
Registration results for the mouse shaped phantom experiment (in units of mm)

Registered central position	
x positive axis	(19.048, 30.895)
x negative axis	(20.392, 30.895)
y positive axis	(21.483, 30.991)
y negative axis	(19.117, 30.991)

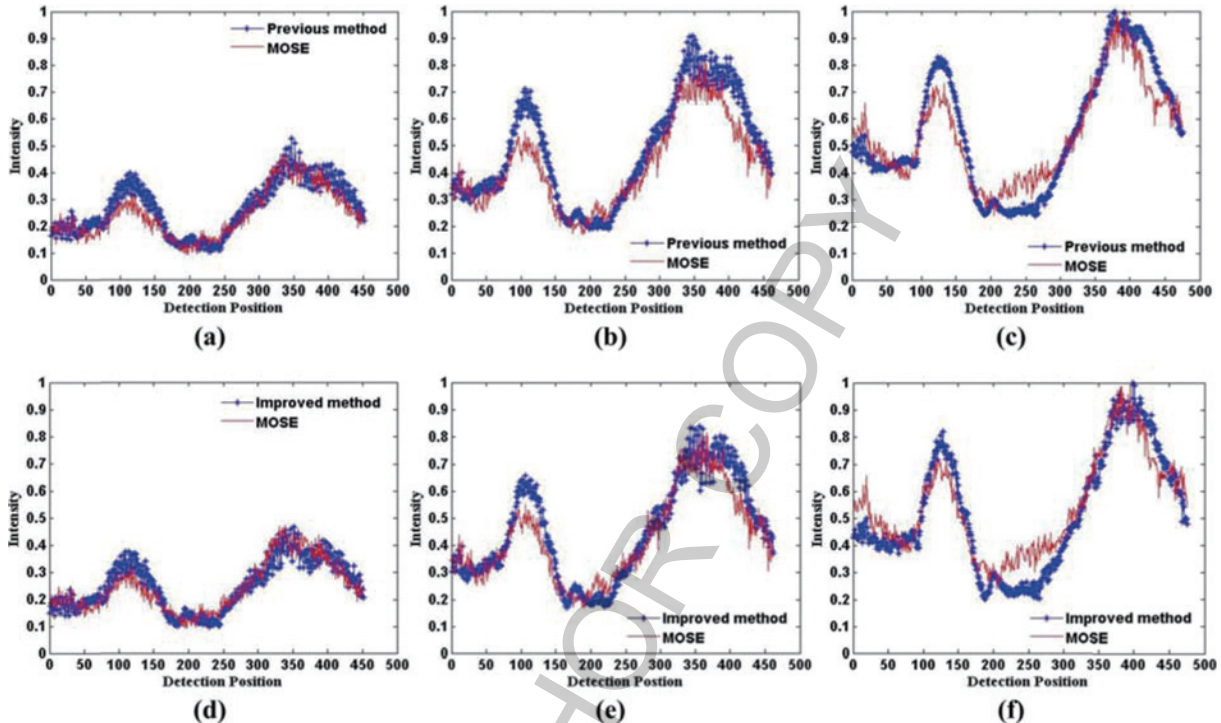


Fig. 5. Comparisons between the recovered light flux distribution on the phantom surface and the simulation results at the height of 14 mm, 17 mm and 20 mm. (a)–(c) Compared curves between the recovered result by our previous proposed method and the simulation one; (d)–(f) Compared curves between the recovered result by the improved method and the simulation one.

and the simulation one, and Fig. 5(d)–(f) present the compared curves between the recovered result by the improved method and the simulation one. The asterisk lines represent the recovered result and the solid lines denote the corresponding simulation result. From Fig. 5, we find that the curves of the improved method approach the simulation ones well at the locations where the previous method did not coincide with the simulation, such as the detection positions 100~150 in Fig. 5(a)–(c) and positions 400~450 in Fig. 5(b) and (c). To quantitatively characterize the improvement, we calculated the recovering error for both the previous and improved method. The recovering error, which can be calculated according to the [20], is 5.4% for our previous method and 4.8% for the improved method which is below 5%. As a result, compared with our previous method, the improved light flux recovering method indeed improved the surface light flux recovering result.

Based on the recovered light flux distribution on the phantom surface by the improved method, the position of the bioluminescent source inside the mouse phantom was reconstructed using the source

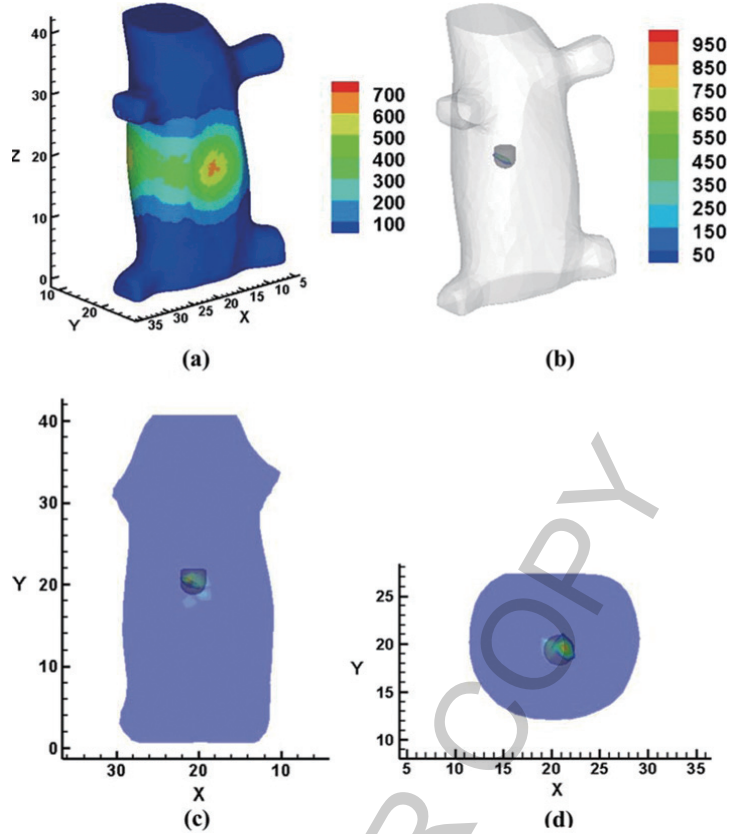


Fig. 6. Performance evaluation of the dual-modality BLT/CT imaging framework. (a) Recovered light flux distribution on the surface of the mouse phantom by using the improved method; (b) 3D view of the reconstructed internal source result; (c) and (d) The corresponding coronal and axial views.

reconstruction algorithm described in Section 3.4. Firstly, the CT volume data of the mouse phantom was discretized into a tetrahedral mesh that is constructed by 9746 tetrahedral elements and 2197 nodes. Then, according to the light flux distribution on the surface of the mouse phantom (as shown in Fig. 6(a)), a potential source region was defined as $\{(x, y, z) \mid 17 < x < 22, 15 < y < 25, 19 < z < 22\}$. Finally, we set up an objective function in the terms of Eq. (8) based on the procedure presented in Section 3.4. Solving the objective function, we obtained the reconstructed position of the internal bioluminescent source as shown in Fig. 6(b)–(d). Therein, Fig. 6(b) presents the 3D view of the reconstructed result, and the corresponding coronal and axial views are presented in Fig. 6(c) and (d). The gray cylinder denotes the actual position of the source that was scanned by the micro-CT sub-system, and the small blue domains represent the reconstructed result. From Fig. 6(b)–(d), we can find that the reconstructed source approaches the actual one well in the case studied. The central position of the reconstructed source is at (21.35, 19.73, 20.55) mm, and the corresponding actual central position is (20.80, 19.52, 20.80) mm, with a distance error being 0.63 mm which is smaller than one step size of light propagation. Thus, the dual-modality BLT/CT imaging framework is of great feasibility and effectiveness, which implemented the dual-modality BLT/CT imaging appropriately.

5. Discussion and conclusion

We have proposed a novel light flux mapping method for dual-modality BLT/CT imaging, which includes two closely-related steps, that is the surface marker based spatial registration and the improved light flux recovering. The spatial registration method is based on the seamless integration of BLT and CT at the system level, and can effectively achieve registration of the 2D BLIs into the coordinate system of the CT volume data. Considering the influence of the camera lens diaphragm, we improved our previously proposed light flux recovering method [20]. Integrating the mapping procedure into the BLT reconstruction, we developed a dual-modality BLT/CT imaging framework, providing a great solution to the dual-modality BLT and CT imaging. Cylindrical phantom based experiments presented the accuracy and effectiveness of the proposed registration method. Using a mouse shape phantom, the performance of the improved light flux recovering method and the potential of the surface light flux mapping method in its application on the dual-modality BLT/CT imaging were also illustrated, which also demonstrated the effectiveness and feasibility of the dual-modality BLT/CT imaging framework. However, there are some deficiencies required that need to be improved. Firstly, the proposed spatial registration method is not universal but specified for the dual-modality BLT/CT imaging framework. This is because the spatial registration method is proposed for and used in conjunction with the surface light flux recovering method. Secondly, the proposed spatial registration method is based on markers labeled on the body surface. The registration accuracy is dependent on the information of the markers, such as the size of the makers, the accuracy of the markers' position, and so on. Thus, this approach is vulnerable to human disturbances. If a marker-free registration method is utilized in our dual-modality BLT/CT imaging framework, human disturbances can be significantly reduced. Lastly, although the improved light flux recovering method provides a better result than our previous proposed method, the improvement is not noticeable. As a result, further improvement of the light flux recovering method is still our interest.

Overall, we have developed a novel dual-modality BLT/CT imaging framework, which will expose new applications of BLT to *in vivo* small animal imaging. These preliminary results show that the proposed registration method and the corresponding dual-modality BLT/CT imaging framework are of great potential and feasibility for the applications of BLT. Further study will focus on the development of the marker free registration method and the new applications of the dual-modality BLT/CT imaging framework.

Acknowledgements

The authors acknowledge the funding supports from the Program of the National Basic Research and Development Program of China under Grant No. 2011CB707702, the National Natural Science Foundation of China under Grant Nos. 81090272, 81101083, 81101084, 81101100, 81000632, 30900334, the Shaanxi Provincial Natural Science Foundation Research Project under Grant No. 2009JQ8018, the Ph.D. programs Foundation of Ministry of Education of China under Grant No. 20090203110002, and Fundamental Research Funds for the Central Universities.

References

- [1] J. Tian, J. Bai, X. Yan, S. Bao, Y. Li, W. Liang and X. Yang, Multimodality molecular imaging, *IEEE Eng Med Biol Mag* **27** (2008), 48–57.

- [2] G. Wang, Y. Li and M. Jiang, Uniqueness theorems in bioluminescence tomography, *Med Phys* **31** (2004), 2289–2299.
- [3] A.D. Klose and B.J. Beattie, Bioluminescence tomography with CT/MRI co-registration, *Conf Proc IEEE Eng Med Biol Soc* **2009** (2009), 6327–6330.
- [4] B.J. Beattie, A.D. Klose, C.H. Le, V.A. Longo, K. Dobrenkov, J. Vider, J.A. Koutcher and R.G. Blasberg, Registration of planar bioluminescence to magnetic resonance and x-ray computed tomography images as a platform for the development of bioluminescence tomography reconstruction algorithm, *J Biomed Opt* **14** (2009), 024045-1–024045-9.
- [5] G. Wang, E. Hoffman, G. McLennan, L.V. Wang, M. Suter and J. Meinel, Development of the first bioluminescent CT scanner, *Radiology* **229** (2003), 566.
- [6] G. Wang, W. Cong, K. Durairaj, X. Qian, H. Shen, P. Sinn, E. Hoffman, G. McLennan and M. Henry, *In vivo* mouse studies with bioluminescence tomography, *Opt Express* **14** (2006), 7801–7809.
- [7] M. Allard, D. Cote, L. Davidson, J. Dazai and R.M. Henkelman, Combined magnetic resonance and bioluminescence imaging of live mice, *J Biomed Opt* **12** (2007), 034018-1–034018-11.
- [8] A.D. Klose, B.J. Beattie, H. Dehghani, L. Vider, C. Le, V. Ponomarev and R. Blasberg, *In vivo* bioluminescence tomography with a blocking-off finite-difference SP₃ method and MRI/CT coregistration, *Med Phys* **37** (2010), 329–338.
- [9] H. Yan, M.B. Unlu, O. Nalcioglu and G. Gulsen, Bioluminescence tomography with structural and functional a priori information, *Proc SPIE* **7557** (2010), 755712-1–755712-6.
- [10] M.A. Naser and M.S. Patterson, Algorithms for bioluminescence tomography incorporating anatomical information and reconstruction of tissue optical properties, *Biomed Opt Express* **1** (2011), 512–526.
- [11] X. Gu, Q. Zhang, L. Larcom and H. Jiang, Three-dimensional bioluminescence tomography with model-based reconstruction, *Opt Express* **12** (2004), 3996–4000.
- [12] W. Cong, G. Wang, D. Kumar, Y. Liu, M. Jiang, L.V. Wang, E.A. Hoffman, G. McLennan, P.B. McCray, J. Zabner and A. Cong, Practical reconstruction method for bioluminescence tomography, *Opt Express* **13** (2005), 6756–6771.
- [13] H. Dehghani, S.C. Davis, S. Jiang, B.W. Pogue and K.D. Paulsen, Spectrally resolved bioluminescence optical tomography, *Opt Lett* **31** (2006), 365–367.
- [14] Y. Lv, J. Tian, W. Cong, G. Wang, W. Yang, C. Qin and M. Xu, Spectrally resolved bioluminescence tomography with adaptive finite element analysis: methodology and simulation, *Phys Med Biol* **52** (2007), 4497–4512.
- [15] S.Ahn, A.J. Chaudhari, F. Darvas, C.A. Bouman and R.M. Leahy, Fast iterative image reconstruction methods for fully 3D multispectral bioluminescence tomography, *Phys Med Biol* **53** (2008), 3921–3942.
- [16] R. Han, J. Liang, X. Qu, Y. Hou, N. Ren, J. Mao and J. Tian, A source reconstruction algorithm based on adaptive hp-FEM for bioluminescence tomography, *Opt Express* **17** (2009), 14481–14494.
- [17] H. Gao, H. Zhao, W. Cong and G. Wang, Bioluminescence tomography with Gaussian prior, *Biomed Opt Express* **1** (2010), 1259–1277.
- [18] X. Chen, X. Gao, X. Qu, J. Liang, L. Wang, D. Yang, A. Garofalakis, J. Ripoll and J. Tian, A study of photon propagation in free-space based on hybrid radiosity-radiance theorem, *Opt Express* **17** (2009), 16266–16280.
- [19] X. Chen, X. Gao, X. Qu, D. Chen, X. Ma, J. Liang and J. Tian, Generalized free-space diffuse photon transport model based on the influence analysis of a camera lens diaphragm, *Appl Opt* **49** (2010), 5654–5664.
- [20] X. Chen, X. Gao, D. Chen, X. Ma, X. Zhao, M. Shen, X. Li, X. Qu, J. Liang, J. Ripoll and J. Tian, 3D reconstruction of light flux distribution on arbitrary surfaces from 2D multi-photographic images, *Opt Express* **18** (2010), 19876–19893.
- [21] J. Liu, Y. Wang, X. Qu, X. Li, X. Ma, R. Han, Z. Hu, X. Chen, D. Sun, R. Zhang, D. Chen, D. Chen, X. Chen, J. Liang, F. Cao and J. Tian, *In vivo* quantitative bioluminescence tomography using heterogeneous and homogeneous mouse models, *Opt Express* **18** (2010), 13102–13113.
- [22] G. Yan, J. Tian, S. Zhu, Y. Dai and C. Qin, Fast cone-beam CT image reconstruction using GPU hardware, *J X-Ray Sci Technol* **16** (2008), 225–234.
- [23] F. Zhu and J. Tian, Modified fast marching and level set method for medical image segmentation, *J X-Ray Sci Technol* **11** (2003), 193–204.
- [24] X. He, J. Liang, X. Qu, H. Huang, Y. Hou and J. Tian, Truncated total least squares method with a practical truncation parameter choice scheme for bioluminescence tomography inverse problem, *Int J Biomed Imaging* **2010** (2010), 291874-1–291874-11.
- [25] H. Li, J. Tian, F. Zhu, W. Cong, L.V. Wang, E.A. Hoffman and G. Wang, A mouse optical simulation environment (MOSE) to investigate bioluminescent phenomena in the living mouse with the Monte Carlo method, *Acad Radiol* **11** (2004), 1029–1038.